Results in Engineering 20 (2023) 101418

Contents lists available at ScienceDirect

Results in Engineering

journal homepage: www.sciencedirect.com/journal/results-in-engineering

Characterization of waste fish bones (*Heteropneustes fossilis* and *Otolithoides pama*) for photocatalytic degradation of Congo red dye

Shyama Prosad Moulick [a,**], Md. Sahadat Hossain [b,*], Md. Zia Uddin Al Mamun [c,***], Farhana Jahan [d], Md. Farid Ahmed [b], Rahima Akter Sathee [c], Md. Sujan Hossen [c], Md. Ashraful Alam [b], Md. Sha Alam [e], Faridul Islam [d]

[a] *BCSIR Laboratories Dhaka, Bangladesh Council of Scientific and Industrial Research (BCSIR), Dhaka-1205, Bangladesh*
[b] *Institute of Glass & Ceramic Research and Testing, Bangladesh Council of Scientific and Industrial Research (BCSIR), Dhaka-1205, Bangladesh*
[c] *Institute of Food Science and Technology (IFST), Bangladesh Council of Scientific and Industrial Research (BCSIR), Dhaka-1205, Bangladesh*
[d] *BCSIR Rajshahi Laboratories, Bangladesh Council of Scientific & Industrial Research (BCSIR), Rajshahi-6206, Bangladesh*
[e] *Institute of Mining, Mineralogy & Metallurgy (IMMM), Bangladesh Council of Scientific & Industrial Research (BCSIR), Joypurhat-5900, Bangladesh*

A B S T R A C T

Heteropneustes fossilis (Shing) and *Otolithoides pama (*Poa) fish bones were chosen as the waste source of photocatalysts which are found in the confined water and the Sea. The bones of these fish are composed of calcium phosphate hydroxide (CPH) which is composed of phosphate and hydroxyl groups and these groups are effective for the photocatalytic activity. The fish bones are characterized by X-ray diffraction (XRD), Field Emission Electron Microscopy (FESEM), Thermogravimetric Analysis (TGA), Differential Scanning Calorimetry (DSC), Fourier-transformed infrared spectroscopy (FTIR), Optical bandgap, Particle size analyzer, etc. Crystallographic information was evaluated using the XRD data focusing on the crystallinity index, lattice parameters, microstrain, crystallite size, dislocation density, degree of crystallinity, β-TCP percentage, HAp percentage, volume fraction of β-TCP, specific surface area, relative intensity, and preference growth. The crystallite size of the natural bones was estimated from the XRD data engaging a number of model equations. Photocatalytic activity of the Shing and Poa fish bones was evaluated by degrading Congo Red dye varying different reaction parameters such as pH, interaction time, catalyst dose, and dye concentration.

1. Introduction

Water pollution, which is getting worse every day, has been an issue and has had a lot of negative consequences on the aquatic ecosystem [1]. The toxic dyes discharged from the industries affect directly the water sources and damage the aquatic environment thus causing a great disorder in the natural growth activity of living organisms [2]. Untreated dyes, of which about 15% are released directly into the environment during the dying process, are extremely harmful to wildlife and plant life [3]. It is imperative to recycle waste to minimize the environmental threat of pollution [4].

Because of the rapid increase in global fishery production, there has been a parallel increase in fish waste generation from fish processing, and it is reported that each year more than 75 megatons of fish waste are produced globally [5]. This huge amount of waste may possess a potential threat to human health through environmental hazards, but this could be valorized in economical and environment-friendly ways as reported in many studies. Some of the applications include the utilization of fish protein hydrolysate derived from fish waste as an organic nitrogen source in algal cultivation [5], use of fish bone as a catalyst in the production of biodiesel via transesterification of used cooking oil [6,7], use of fish bone to produce biomedical appliances [8,9] etc.

In recent times, there has been a notable demand for cheaper photocatalysts derived from biological waste for the decomposition of industrial synthetic poisonous dyes before their discharge into the water bodies [10]. Fishbone, since composed mostly of inorganic hydroxyapatite, reportedly has a promising application in this field [11]. It is used to extract and synthesize natural hydroxyapatite, which has the capacity to act as a photocatalyst to remove toxic metal ions and thus bleach the wastewater [12–16].

In today's world, the demand for clean water is on the rise due to dramatic increase in water pollution through rapid industrialization and

* Corresponding author.
** Corresponding author.
*** Corresponding author.
E-mail addresses: moulik.shyama@bcsir.gov.bd (S. Prosad Moulick), saz8455@gmail.com (Md. Sahadat Hossain), ziaalmamun.du@gmail.com (Md. Zia Uddin Al Mamun).

https://doi.org/10.1016/j.rineng.2023.101418
Received 28 July 2023; Received in revised form 20 August 2023; Accepted 14 September 2023
Available online 16 September 2023

Table 1
Local, common names, and scientific names of the selected fish samples.

Local Name	English/Common Name	Scientific Name
Shing Mach	Asian stinging catfish	*Heteropneustes fossilis* (Hamilton, 1822)
Poa Mach	Pama Croaker	*Otolithoides pama* (Hamilton, 1822)

urbanization and it is alarmed that the number of global people living in water scarce areas will increase to 4 billion by the next decade, which provides a clear message about the immediate need for wastewater treatment [17]. Nowadays, textiles, plastics, leather, food processing, medicine, pharmaceutical, paper, cosmetics and rubber industries are discharging toxic dyes in the effluents causing threat to aquatic creatures, disturbing aquatic ecosystem and public health [18] Textile industries directly discharge different deeply colorful synthetic dyes into the water systems, which are toxic, mutagenic and non-biodegradable. Because of such problematic nature of the dyes, the wastewater demands urgent treatment for the elimination of the dyes before being discharged [19]. Several methods are available for the degradation and removal of the harmful wastewater dyes including precipitation, membrane filtration, flotation, coagulation, ion exchange, irradiation, adsorption and photocatalysis etc. [1] In a recent study in Bangladesh, silver carp fish bone has been reported to be an effective bioadsorbent for the removal of carcinogenic anionic Congo red dye from synthetic wastewater solution [20].Pretreated fish bone may also be effectively used as a proper adsorbent for the removal of cationic dye from aqueous solutions [21]. However, photocatalysis is known as the cheapest and a simple designed process in elimination of dyes from wastewater [18,22].

Stinging catfish (*Heteropneustes fossilis*), locally known as Singhi, is a highly consumed indigenous freshwater catfish with easily digestible high quality protein, high calcium and iron content and therapeutic value which is widely cultured in Bangladesh [23–25]. Besides, pama croaker (*otolithoides pama*), also known as poa, is a marine croaker species commonly consumed in Bangladesh which is quite rich in protein and minerals [26]. Because of the abundance, the bones from Shinghi and poa were used in the present study for the removal of dyes from wastewater through a photocatalytic mechanism as part of their bio-waste management.

In this research two types of fish bones were characterized from a crystallographic view point and evaluated their photocatalytic degradation of Congo red dye.

2. Materials and methods

2.1. Collection of the selected fish samples

Two species of fish (one freshwater and one marine fish species) were selected for the study. The fish samples were collected from Jatrabari, Dhaka, Bangladesh wholesale fish market, one of the largest fish markets in Dhaka, Bangladesh. The samples were kept in an ice box (HDPE ice box, India) with each type of sample in a separate sterile iced polythene bag to avoid any types of contamination and then transported it to the Fish Technology Research Laboratory of the Institute of Food Science and Technology (IFST), BCSIR, Dhaka. It took approximately one and half hours (1.5 h) for the transportation of the samples from Jatrabari to the designated lab. The characteristics of the fish samples including their local names, common names, and scientific names have been represented in Table 1.

2.2. Chemicals and Equipment's used

All the chemicals required for the analyses were of analytical grade, procured from E-Merck (Darmstadt, Germany), and used exactly as they were received. Analytical grade Congo red (chemical formula: $C_{32}H_{22}N_6Na_2O_6S_2$; molar mass: 696.665 g/mol; $\lambda_{max} = 498$ nm), an azo dye was used in the experiment to have an insight on the dye degradation properties of the fish bones powder. Deionized water was used throughout the study for cleaning as well as other purposes. The glassware used in this experiment was of Pyrex, England brand due to its resistance to breakage during extreme shifts in temperature or electricity. Sophisticated instruments namely WDXRF, FT-MIR and FE-SEM have been employed for the characterization of fish bone powder. Minerals were analyzed using a flame photometer (LX406FP, LABDEX, UK). Ultraviolet–visible (UV-VIS) spectrophotometer (SHIMADZU UV-1800) was used to enumerate the photolytic dye degradation activity of the fish bone powder through its absorbance measurement.

2.3. Preparation of fish bone

The collected fish samples were labeled based on their species name and kept in a refrigerator (SJC-328-GY, Sharp, Japan) at −20 °C until analysis. The samples were cleaned with tap water followed by one with distilled water and de-gutted with a sterile, stainless-steel knife. The cleaned, de-gutted samples were boiled in 100 °C water for about 1.5 h for the removal of scales, skin, meat, and traces of viscera. Then the defleshed fish bones were repeatedly washed with hot distilled water to remove the constituents like proteins, fat, and other organic impurities. Thereafter, the bones were dried in an oven at 65 °C for about 5 h. The dried bones were crushed into pieces small enough to take into a porcelain crucible and calcined in a muffle furnace at 900 °C for 2 h. Finally, the calcined bones were pulverized with a mortar pestle into a fine powder and kept in an airtight container (stored at 4 ℃) for further analyses.

2.4. X-RD analysis of fish bone

To have an insight into the crystallographic information including phase purity, crystal grain size, degree of crystallinity, dislocation density, microstrain, crystallinity index, and change in the crystallinity of the fish bone powder was enumerated using an X-ray diffractometer (PAN alytical X'pert PRO XRD PW 3040) with radiation source from mono chromate Cu-Kα (λ = 1.54060). The standard data JCPDS (Joint Committee on Powder Diffraction Standards) was selected here to make a comparison with the synthesized fish bone powder calcium phosphate data.

2.5. Morphological characterization

To observe the surface morphology and microstructure of the two types of fish bones, the field emission scanning electron microscopy (FE-SEM) (Zeiss FE-SEM Sigma 300) technique was adopted which is equipped with EDX facilities that help unravel the chemical composition of the fish bone samples.

2.6. Thermogravimetric analysis (TGA)

Under a nitrogen environment and at a heating rate of 10 K/min, a NETZSCH STA 449 F5 simultaneous thermal analyzer (STA) was used to conduct thermogravimetric analysis (TGA) and differential scanning calorimetry (DSC). The analysis was done before the calcination of the sample from room temperature to 1200 °C.

2.7. FTIR analysis

Fourier-transformed infrared spectroscopy (FTIR) was carried out to identify the presence of functional groups in the fishbone powders. The sample was kept in on the ATR (attenuated total reflection)crystal of ATR-FTIR (Spectrum, PerkinElmer, USA). The spectra were recorded with a scan range of 500–4000 cm^{-1}.

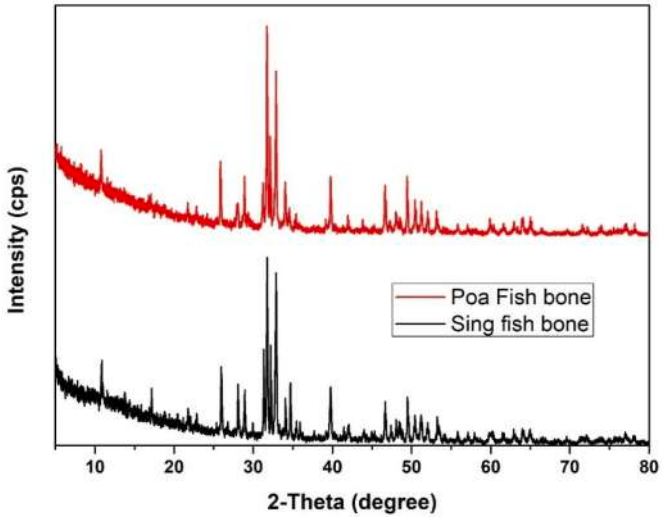

Fig. 1. XRD of Shing and Poa fish bones.

2.8. UV–Vis spectrophotometer

The energy required for the electronic transition from valence band to the conduction band was estimated employing UV–Vis-spectrophotometer (Shimadzu, Japan, model: U-2900) machine which was operated at room temperature and at a relative humidity of 50~60%.

2.9. Particle size analysis

A nanoparticle analyzer machine (Model: Horiba Scientific, Nano Partica, SZ-100V2) was engaged to estimate the particle size of the two types of fish bones. The machine was operated at 100 mW laser and the size of the particles was estimated following dynamic light scattering (DLS) method.

2.10. Photocatalytic efficiency

A stock solution of 1000 ppm was prepared to dissolve the required amount of Congo red into a certain amount of de-ionized water. A varying concentration of Congo red dye solution was prepared by diluting the prepared stock solution of Congo red with distilled water. The photocatalytic experiment was conducted under sunlight irradiation on different days in the month of February/March 2023 between 10 a.m. and 4 p.m. in Bangladesh local time. The sample solution was stirred in a magnetic stirrer at 250 rpm for about 10 min and kept in direct exposure to the sunlight until the solution turned colorless. At an interval of every 1.0 h the samples were taken for absorbance measurement using Ultraviolet–visible (UV-VIS) spectrophotometer (SHIMADZU UV-1800) before spinning in a centrifuge (Thermo Scientific,21 R). The only dye solution was chosen as a control for the experiments.

3. Results and discussion

3.1. XRD analysis (crystallographic analysis)

The X-ray diffraction (XRD) pattern of the two types of calcined fish bones is illustrated in Fig. 1. These two types of bones presented very similar types of patterns which were matched with the standard ICDD database (card no# 01-082-2956) of calcium phosphate hydroxide (CPH). Crystallographic characterization of the natural fish bones was evaluated focusing the crystallinity index, lattice parameters, microstrain, crystallite size, dislocation density, degree of crystallinity, β-TCP percentage, HAp percentage, volume fraction of β-TCP, specific surface area, relative intensity, and preference growth. The mathematic

Table 2
Comparative table of d-spacing, intensity, lattice parameters, and unit cell volume.

Lattice parameters of standard (card# 01-082-2956)		Lattice parameters and experimental data of natural fish bones				h k l
ICDD		Sing Fish bone		Poa Fish bone		
d-spacing	Intensity (I) (%)	d (Å)	I (%)	d (Å)	I (%)	
2.812	100	2.8155	100	2.8183	100	2 1 1
2.777	50	2.7765	30	2.7831	32	1 1 2
2.717	59	2.7213	89	2.7225	86	3 0 0
a = b = 9.415 Å, c = 6.879 Å V = 528.14 Å		a = b = 9.427 Å, c = 6.87 Å V = 528.73 Å		a = b = 9.431 Å, c = 6.89 Å V = 530.76 Å		

explanations are presented in equations (1)–(12) [27].

$$\text{Crystallinity index, } CI_{XRD} = \sum \frac{H_{(202)} + H_{(300)} +) + H_{(112)}}{H_{(211)}} \quad (1)$$

$$\text{Lattice parameter equation, } \left(\frac{1}{d_{hkl}}\right)2 = \frac{4}{3}\left(\frac{h^2 + hk + k^2}{a^2}\right) + \frac{l^2}{c^2} \quad (2)$$

$$\text{Microstrain, } \varepsilon = \frac{\beta}{4\tan\theta} \quad (3)$$

$$\text{Crystallite size, } D_c = \frac{K\lambda}{\beta\cos\theta} \quad (4)$$

$$\text{The Dislocation density, } \delta = \frac{1}{(D_c)^2} \quad (5)$$

$$\text{Degree of Crystallinity, } Xc = \left(\frac{Ka}{\beta}\right)(\hat{3}) = \left(\frac{0.24}{\beta}\right)(\hat{)}3 \quad (6)$$

$$\text{Percentage of } \beta - TCP = \frac{I_{\beta-TCP(0210)}}{I_{HA(211)} + I_{\beta-TCP(0210)}} \quad (7)$$

$$\text{Percentage of CPH} = \frac{I_{HA(211)}}{I_{HA(211)} + I_{\beta-TCP(0210)}} \quad (8)$$

$$\text{Volume fraction of } \beta - TCP, X_B = \frac{PW_B}{1 + (P-1)W_B} \quad (9)$$

$$\text{Specific surface area, } S = \frac{6 \times 10^3}{\rho \times D_c} \quad (10)$$

$$\text{Relative intensity, } RI = \frac{I_{(211)}}{I_{(300)} + I_{(112)} + I_{(202)}} \quad (11)$$

$$\text{Preference growth, } P = \frac{RI_s - RI_{st}}{RI_{st}} \quad (12)$$

Here, K= Scherrer constant, FWHM = β = full width at half maxima, a, b, c, h, k, l are the lattice parameters, $H_{(hkl)}$ = peak height, K_a = constant, $I_{\beta\text{-TCP}(0210)}$ = intensity of β-TCP at (0210), P = 2.275 =

Table 3
Crystallographic information of the Shing and Poa fish bones.

Parameter	Shing bone	Poa bone
Crystallinity index, CI_{XRD}	1.61	1.39
Crystallite size, nm	93	82
Microstrain, ε	0.09	0.08
CPH percentage	65.45	87.78
Dislocation density, (10^{15} lines/m^2)	0.115	0.148
Degree of crystallinity	11.27	18.96
Volume Fraction of β-TCP	0.54	0.24
β-TCP percentage	34.55	12.22
Specific surface area, S	20.54	23.30

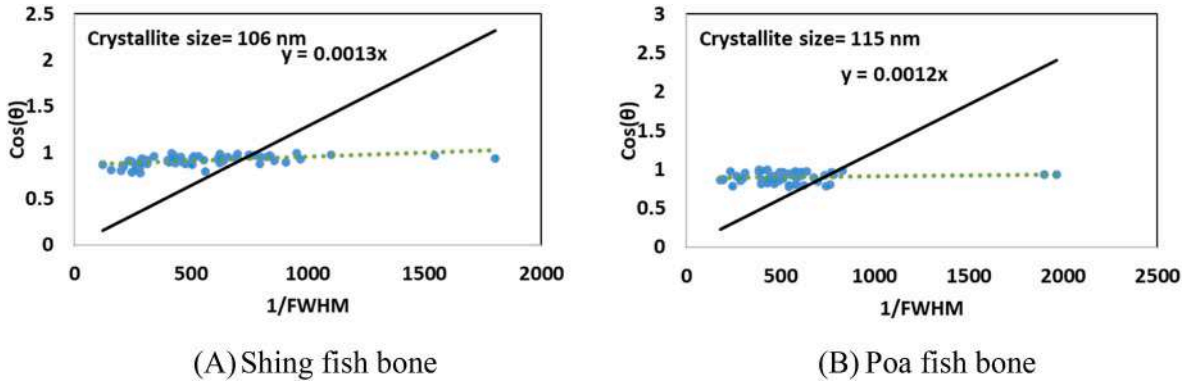

Fig. 2. Estimation of crystallite size from Sahadat-Scherrer model.

combined intensity of the CPH and β-TCP, W_B = β-TCP percentage.

A comparative table of the lattice parameters, unit cell volume and the relative intensity of the standard and two types of fish bones are presented in Table 2.

The crystallinity index, lattice parameters, microstrain, crystallite size, dislocation density, degree of crystallinity, β-TCP percentage, HAp percentage, and volume fraction of β-TCP of the two types of fish bones were calculated and registered in Table 3. All the parameters of the two types of fish bones relatively similar, though there remained a slight variation. CPH percentage in the case of river fish bones are relatively lower than the sea fish bones which may be due to the presence of different types of salt in the sea water.

To estimate the preference growth of a certain plane, relative intensity is required which can be calculated from equation (11). The relative intensity of a plane (e.g. 211 plane) can be estimated considering other three plane (e.g. 300, 112, and 202 planes) and is revealed as in equation (11). From the relative intensity of the sample (RI_s) and standard (RI_{st}), the preference growth of a certain plane can be estimated. For the Shing and Poa fish bones the preference growth of the plane 211 against 300, 112, and 202 planes are −0.10, are −0.06, respectively. The negative sign of the preference growth indicated the thermodynamically unfavorable plane (211) of the most intense peak of the river and sea fish bones.

3.1.1. Crystallite size calculation using models

Different models have been employed to estimate the crystallite size of the two types of fish bones and few of the models widely used are the Sahadat-Scherrer model, Monshi–Scherrer method, straight line method, Uniform deformation model, Stress deformation model, and Energy deformation model.

3.1.2. Sahadat-Scherrer model

The crystallite sizes of the two types of natural fish bones were calculated from the Sahadat-Scherrer model which is mathematically expressed as equation (13) [28]. The details of the equation can be found in the published literature [29]. Fig. 2 represents the Sahadat-Scherrer model of Shing and Poa fish bone.

$$\text{Sahadat} - \text{Scherrer model}, \cos\theta = \frac{K\lambda}{D_{S-S}} \times \frac{1}{\beta} \tag{13}$$

The crystallite sizes calculated from this model were 106, and 115 nm for Shing fish bone and Poa fish bone, respectively. As the crystallite sizes was relatively small it can be said that this model is applicable for the estimation of crystallite size of river fish bone (Shing fish) and sea fish bone (Poa fish). The value was also close to the crystallite size calculated from the Scherrer equation.

3.1.3. Monshi–Scherrer's method

The Monshi-Scherrer model is another widely applicable model for the computation of crystallite size from the powder XRD data. This model was built by putting 'ln' on each side of the Scherrer equation (equation (4)) and mathematically presented as equation (14) (details are presented elsewhere) [29,30]. Fig. 3 visualized the Monshi-Scherrer method to estimate crystallite size for Shing and Poa fish bones.

$$\text{Monshi–Scherrer method}, \ln\beta = \ln\frac{1}{\cos\theta} + \ln\frac{K\lambda}{D_M} \tag{14}$$

The crystallite sizes of Shing and Poa fish bones were 119 and 76 nm, respectively, calculated from the Monshi-Scherrer model. These values were also relatively small and nearly close to each other as well as the previously mentioned model.

3.1.4. Straight line method of Scherrer's equation

Straight line method of Scherrer's equation (Fig. 4) is another way to measure the crystallite size where the Scherrer equations is utilized to

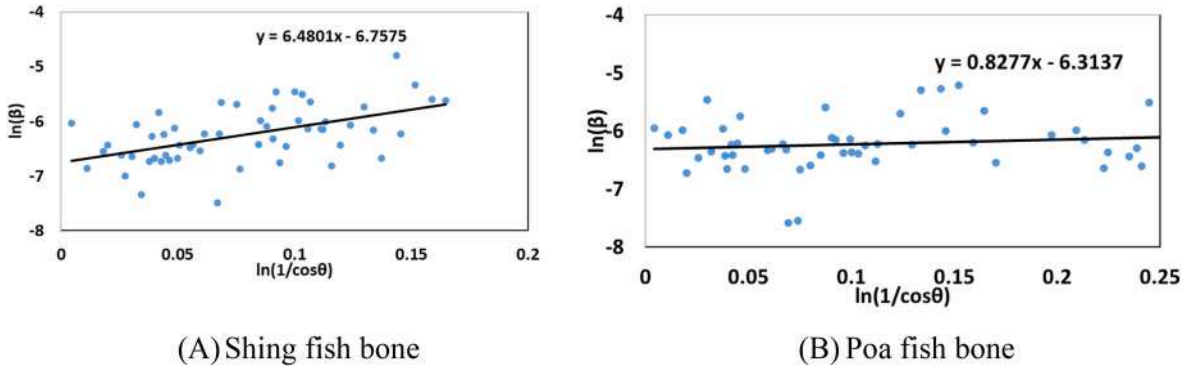

Fig. 3. Calculation of crystallite size from Monshi-Scherrer model.

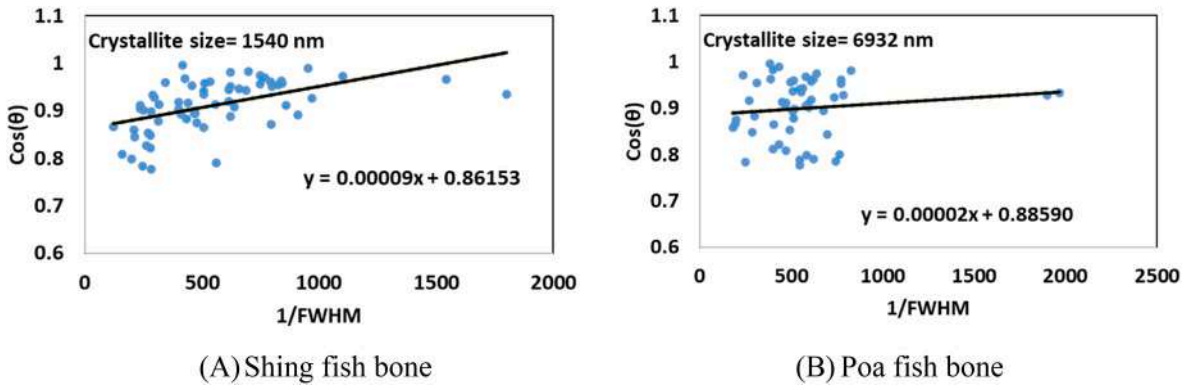

Fig. 4. Measurement of crystallite size from the Straight line method of Scherrer's equation.

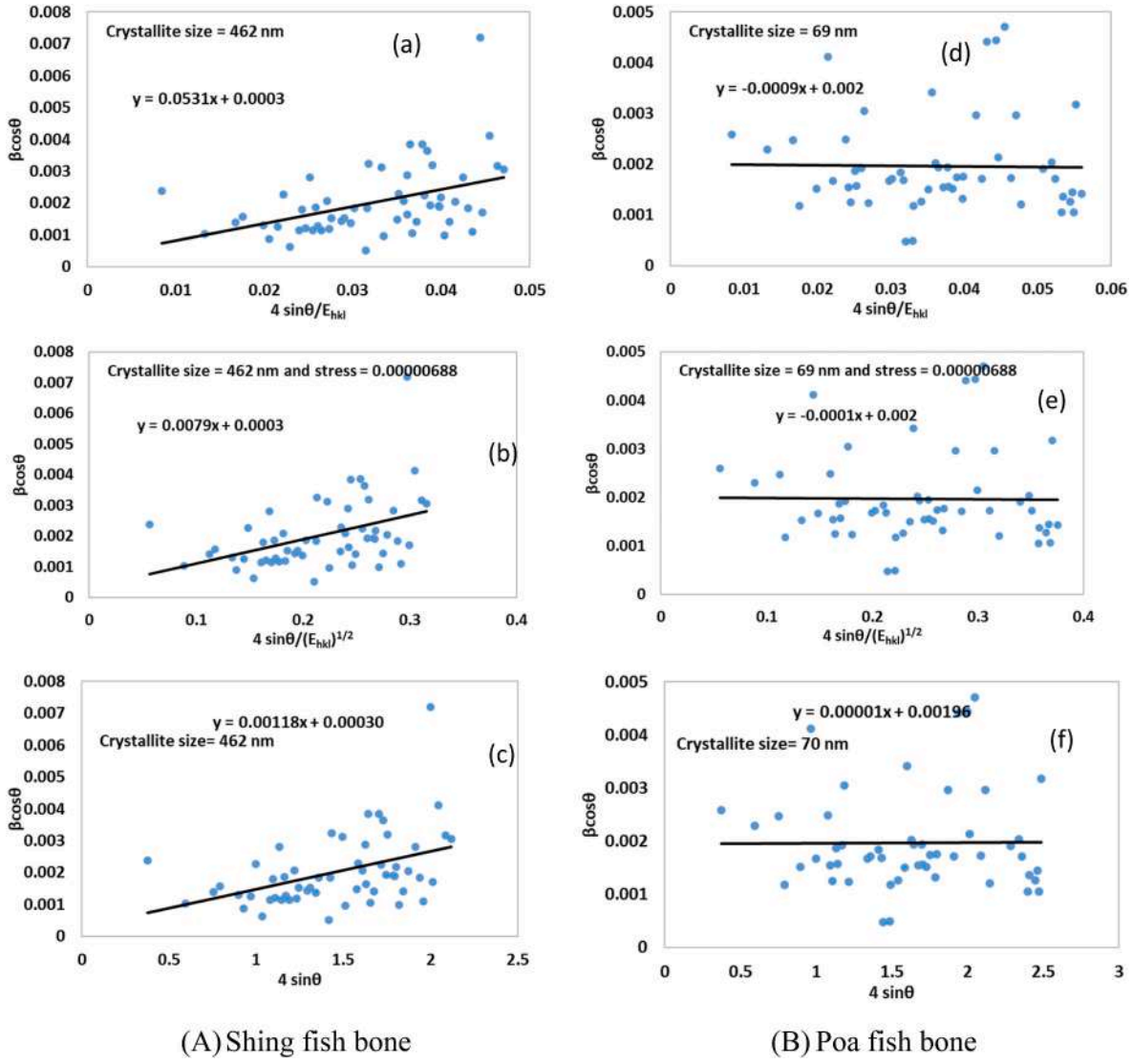

Fig. 5. Estimation of crystallite size of Shing fish bone using (a) Uniform Stress Deformation Model, (b) Uniform Deformation Energy Density Model, (c) Uniform Deformation Model, and of Poa fish bone using (d) Uniform Stress Deformation Model, (e) Uniform Deformation Energy Density Model, (f) Uniform Deformation Model.

build a straight line. Equation (15) is utilized to compute the crystallite size and the details of the model is described elsewhere [28].

Straight line method of Scherrer's equation

$$\cos\theta = \frac{K\lambda}{D_c} \times \frac{1}{\beta} = \frac{K\lambda}{D_L} \times \frac{1}{\beta} \tag{15}$$

The crystallite size calculated from this model is very high that is

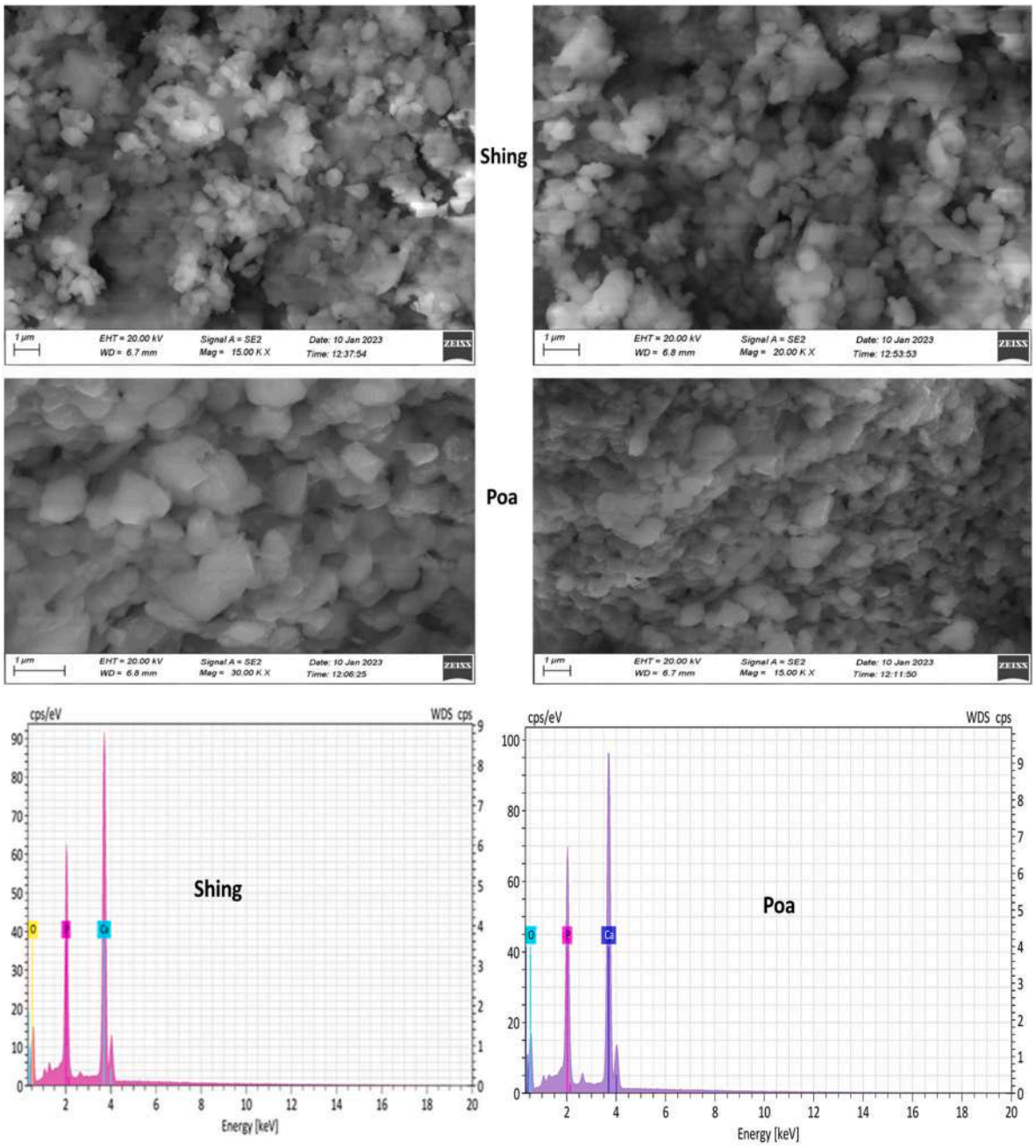

Fig. 6. FESEM and EDX of the Shing and Poa fish bones.

1540 and 6932 nm for Shing and Poa fish bone. But this high value of crystallite size cannot be accepted for the natural fish bones. So it can be said that this model is not valid for the analyzed samples.

3.1.5. *Williamson–Hall method*

Considering the intrinsic strain, the crystallite size can be calculated using Williamson-Hall method (Fig. 5). This model can be expressed as Uniform Stress Deformation Model (USDM), Uniform Energy Density Model (USEDM) and Uniform Deformation Model (UDM), and the mathematical form of these models are presented in equations (16)–(18). The details of these model can be found elsewhere [31–33].

The Uniform Stress Deformation Model (USDM):

$$\beta_{total}\cos\theta = \frac{K_B\lambda}{D_{W-H}} + 4\,\frac{\sigma}{E_{hkl}}\sin\theta \tag{16}$$

The Uniform Deformation Energy Density Model (UDEDM):

$$\beta_{total}\cos\theta = \frac{K_B\lambda}{D_{W-H}} + 4\left(\frac{2u}{E_{hkl}}\right)^{1/2}\sin\theta \tag{17}$$

The Uniform Deformation Model (UDM):

$$\beta_{total}\cos\theta = \frac{K_B\lambda}{D_{W-H}} + 4\,\varepsilon\sin\theta \tag{18}$$

For the Shing fish bone, the crystallite size is very high which made these model invalid for Shing bone but small crystallite sizes were found for the Poa fish bone.

3.2. *Field emission scanning electronic microscopy (FESEM)*

FE-SEM was used to analyze fish bones powder morphology and structure prepared from the fishbone of species *Heteropneustes fossilis* (Shing) and *otolithoides pama* (Poa) which are shown in Fig. 6. While

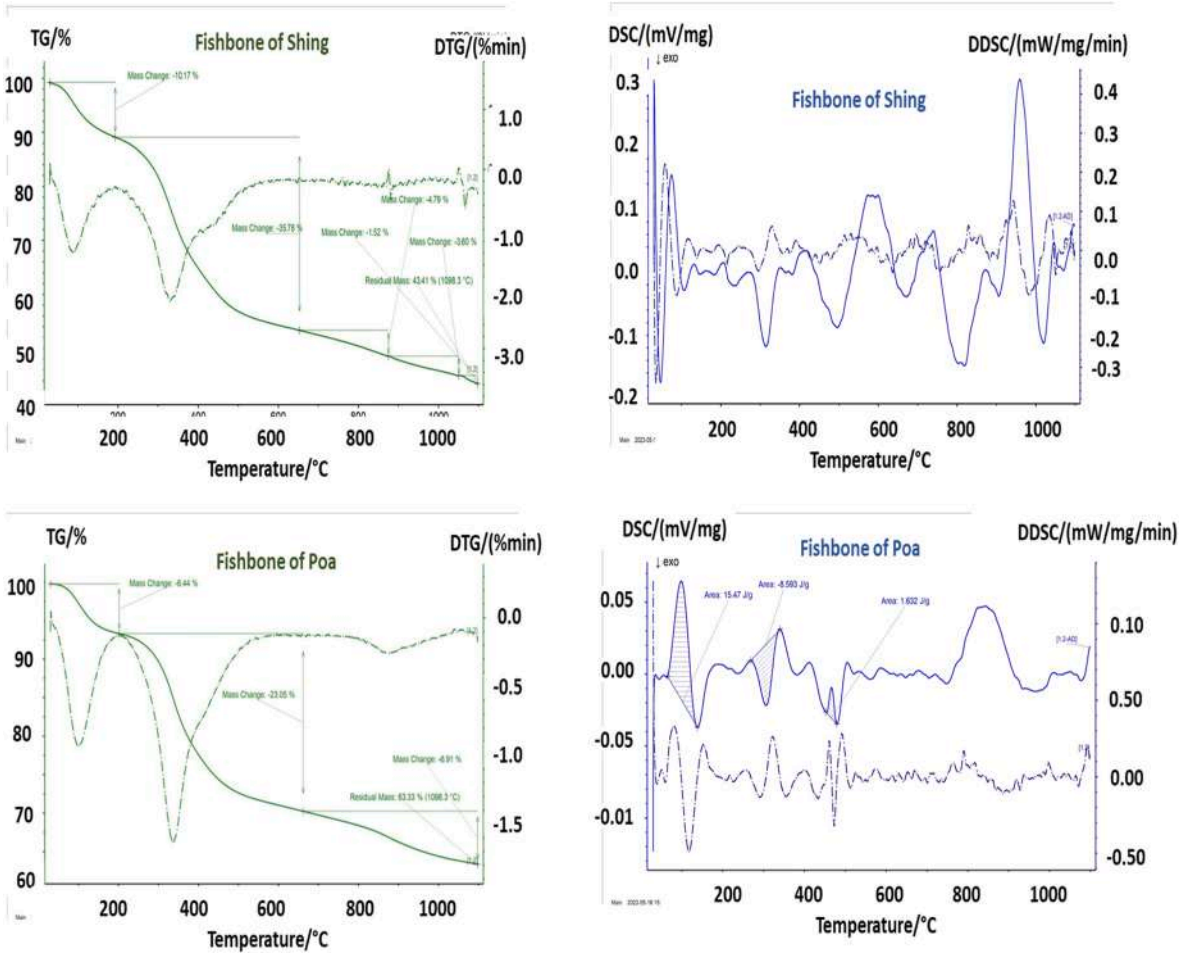

Fig. 7. TGA and DSC curve for fishbone of Shing and Poa.

synthetic hydroxyapatite occurs in a variety of sizes and shapes, including spheres, sponges, and rectangles, only sphere-shaped particles were observed in natural fish bones, regardless of river or sea of origin. The mechanism of hydroxyapatite crystal nucleation and growth will be influenced by temperature. With a rise in temperature, the amount of Ca^{2+}, OH^{-}, and PO_4^{-3} in the core will increase quickly, leading to the growth of a large amount of core and the production of agglomerates [34]. In addition, the percentages and the presence of elements on the fishbone of Shing and Poa fish were analyzed with the help of EDX (Fig. 6). The mass percentages of Ca, O, and P contained in the synthesized CPH from the fishbone of the Shing were 46.86, 40.32, 12.82, and whereas in the fishbone of Poa were 46.13, 40.17, and 13.70, respectively. By using a flame photometer (LX406FP, LABDEX, UK), the calcium content was also calculated. The calcium content in the fish bones from Shing and Poa was determined by using a flame photometer (LX406FP, LABDEX, UK) and found to be 39.05% and 37.32% respectively, which is approximately consistent with the data collected from EDX. The data obtained from FTIR data and XRD has not revealed any other elements except Ca, O, and P. Hence, it is conceivable to foresee that the fish bones contained no additional material.

3.3. TGA analysis

The decomposition pattern of the bone was investigated from Fig. 7 Loss of interstitial water led to an initial loss of weight of around 10.17% and 6.44% for Shing and Poa respectively, in the range of 30–205 °C, as demonstrated by an endothermic peak in the DSC curve at this region. In the range of 205 and 600, considerable weight loss occurred as a result

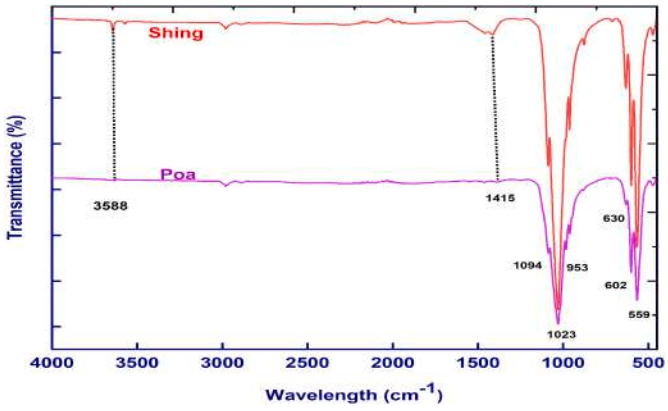

Fig. 8. FTIR spectra of fish bone of Shing and Poa.

of the breakdown of organic molecules. When heated to temperatures between 280 °C and 590 °C, shing and poa lose roughly 35.78 and 23.05% of their weight, respectively. Shing and Poa have respective residual masses of 43.41 and 63.33%.

3.4. FTIR analysis

The FTIR spectra of the fishbone of Shing and Poa were shown in Fig. 8. Both spectra show a sharp peak at 1023 and 1094 cm^{-1} which is due to the asymmetric stretching vibration of O–P of the PO_4^{3-} whereas

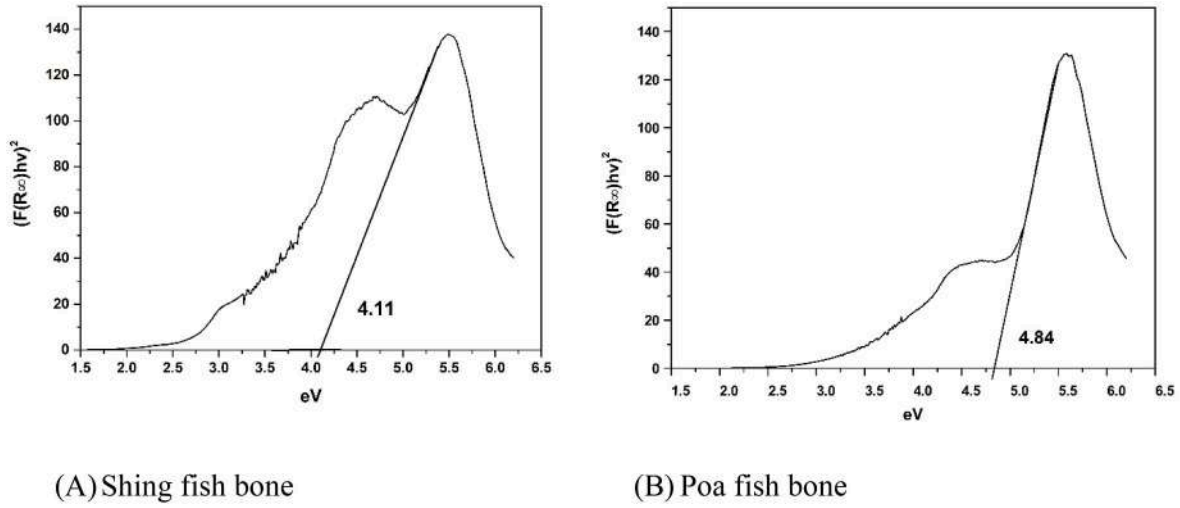

Fig. 9. Bandgap energy of the Shing and Poa fish bones.

the peak at 953 cm^{-1} symmetric mode of vibration. The two less intense peaks at 602 and 559 cm^{-1} denote the bending vibration mode of the phosphate group. FTIR spectrum of Shing showed a more intense peak near 3500 cm^{-1} which of O–H stretching and a peak at 630 cm^{-1} is due to the O–H contraction mode of the hydroxyl group. The peak at 1415 cm^{-1} might be due to the substitution of the PO_4^{3-} by the CO_3^{2-} of Carbonate CPH. All the characteristic peak in the spectra obtained from FTIR analysis of fishbone of shing and poa is similar to the previously reported spectra of CPH where phosphate plays a vital role during the degradation of dye [18].

3.5. Band gap energy

Optical bandgap energy of the Shing and Poa fish bone were calculated from the electronic transition of valence band (VB) to conduction band (CV). P. Kubelka and F. Munk theory was employed to obtained the data in the absorbance form then the optical bandgap was estimated form the Tauc plot following equations 19–21. The details of the methods can be found in published literature [29] and Fig. 9 illustrates the optical bandgap of Shing and Poa fish bones. The Band gap energies for Shing and Poa fish bones were 4.11 and 4.84 eV, respectively.

$$\propto h\vartheta = A\left(h\vartheta - E_g\right)^n \tag{21}$$

$$F(R_\infty) = \frac{K}{S} = \frac{(1-R_\infty)^2}{2R_\infty} \tag{22}$$

$$F(R_\infty)\ h\vartheta = A\left(h\vartheta - E_g\right)^n \tag{23}$$

here ν = photon's frequency, h = Planck constant, A = constant, Eg = band gap energy, K = absorption coefficient, R_∞ = reflectance at infinity, S = scattering coefficient.

3.6. Particle size analysis

The size of the particle of the CPH produced from the fishbone of Shing and Poa was analyzed using a Nanoparticle Size Analyzer (nanoParticaSZ-100-S2, HORIBA scientific ltd, Japan) at 25.1 °C following the dynamic light scattering method. The size of the particle was found to be 1964.4 nm and 2638.8 nm for the fishbone of Poa and shing respectively.

3.7. Photocatalytic activity

The photocatalytic activity of the catalyst CPH (Poa) and CPH (Shing) was performed under direct irradiation of sunlight where Congo red was used as a dye. The degradation percentage (D_p) was calculated using the equation, $D_p = (C_0\text{-}C_{HAp})/C_0$ Where C_0 is the concentration of dye and C_{HAp} is the concentration of the solution containing catalyst. At first, the dose of catalyst was optimized for further analysis of photocatalytic activity keeping constant dye concentration at 1hr, and the degradation percentage (DP) was presented in Fig. 10 (a). The figure showed that with increasing the catalyst weight, the DP also increased

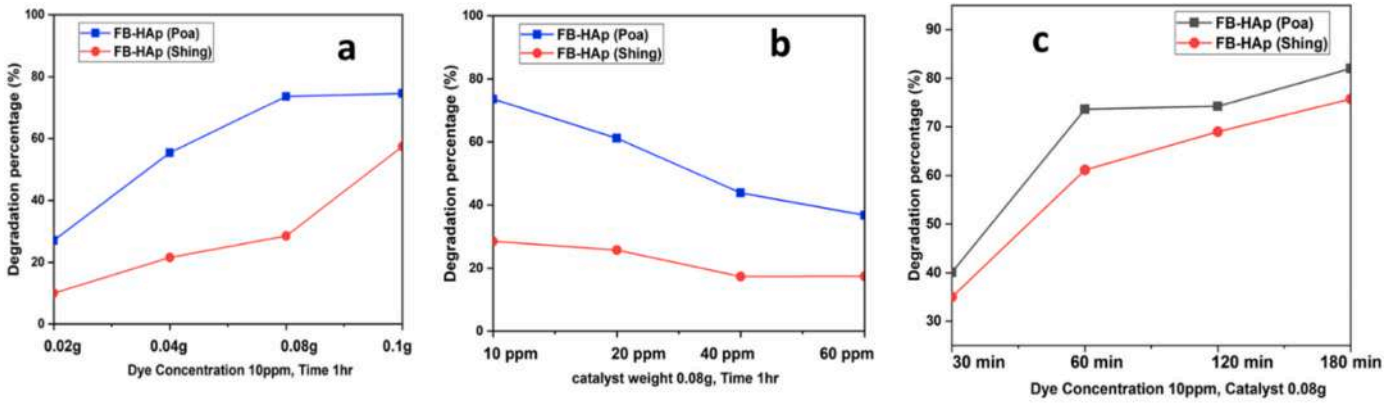

Fig. 10. Degradation percentage with a variation of catalyst weight (a), dye concentration (b), time (c).

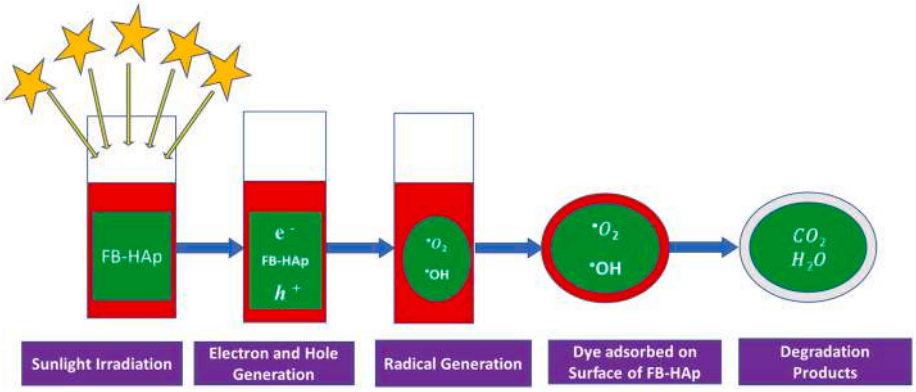

Fig. 11. Photocatalysis degradation process.

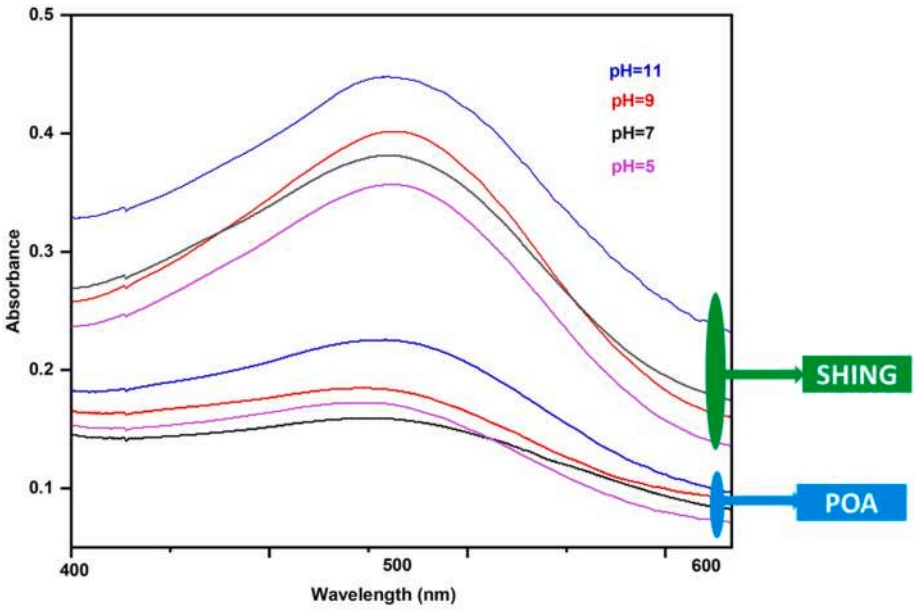

Fig. 12. P^H variation curve for photo degradation.

for both the fishbone and the degradation percentage for the 0.1 g and 0.08 g catalysts were maximum. Considering the suitability of a lower dose 0.08 g catalyst dose was chosen from here for performing the analysis.

Then the DP was measured after 1hr from the mixing time of 0.08 g of catalyst to the 50 mL of dye solution having different concentrations (10 ppm, 20 ppm, 40 ppm, and 60 ppm). And the DP was found to be high for both the fishbone of poa and shing when 10 ppm Congo red was used (Fig. 10 (b)). At last, the photocatalytic activity was monitored at different time intervals (30 min, 60 min, 120 min, and 180 min) using a 0.08 g of catalyst and a 10.0 ppm solution of dye and the results of the photocatalytic degradation were given in Fig. 10(c). The degradation percentage for both catalysts increased with time but the catalyst CPH (Poa) degraded a greater amount of dye than CPH (Shing) and reached the maximum degradation percentage (almost 82%) whereas the catalyst CPH (Shing) degraded a maximum of 73% of the dye within 3 h.

From the figure, it can be seen that the DP value after 1st hr was not found to be changed significantly. So CPH (Poa) could be a more potential source than CPH (Shing) to play a significant role in azo dye removal during wastewater treatment. The tentative mechanism of photocatalytic degradation of azo dyes using CPH is much more popular and given by the following Fig. 11 [1,18].

Superoxide anion radical ($O_2^{\cdot}$) and hydroxyl radical (HO.) were created from O_2 and H_2O molecules through interactions between the negative charge of the electrons and the positive charge of the mesoporous holes. The produced negatively active free radical is strongly bound with the positive hole. Then the adsorbed molecules of Congo dye are broken down into CO_2 and H_2O by these active species of CPH [18]. The degradation of Congo dye was observed for optimized composition after 1hr which was given in Fig. 12. From the curve, it can be seen that both the fishbone provided a greater degradation at neutral (pH = 7) and slightly acidic conditions (pH = 5). However, the absorbance at 498 nm for the fishbone of shing was higher for every medium condition (acidic, basic, and neutral) compared to the fishbone of Poa which indicates the greater degradation capacity for the fishbone of Poa. The figure also showed the slight shifting of the position of maximum absorbance to the right direction of wavelength i,e bathochromic shift with the increasing of pH value of the medium.

4. Conclusion

Photocatalytic degradation of textile effluent is one of the most efficient methods of wastewater treatment. Nano-crystallite waste fish bone can be utilized as an efficient photocatalyst for the degradation of Congo Red dye. The utilization of waste fish bones will reduce the environmental pollution and add new low cost photocatalyst for the

degradation of textile effluent. The crystallographic characterization of waste Shing and Poa fish bone will open new ways of application in different fields will minimize the environmental pollutant. From this research it is suggested to use waste fish bones for photocatalytic degradation of textile effluent (Congo Red dye).

Authors contribution

Shyama Prosad Moulick: Carried out the photocatalytic experiment, analyzed the data, arranged all the experimental facilities, and wrote the draft. Md. Sahadat Hossain: Performed the crystallographic data analysis, analyzed the experimental data, wrote the original manuscript, and corrected the final manuscript. Md. Zia Uddin Al Mamun: Performed the photocatalytic experiment, analyzed the data, arranged the required facility with financial support. Farhana Jahan: Estimated the calcium (Ca) content and performed the FT-IR experiment. Md. Farid Ahmed: Carried out the TGA, Particle size and UV–Vis analysis. Rahima Akter Sathee: Carried out the photocatalytic experiment. Md. Sujan Hossen: Assisted in photocatalytic experiment. Md. Ashraful Alam: Executed the XRD analysis. Md. Sha Alam: Contribution in FE-SEM and EDX analysis. Faridul Islam: Contributed in FE-SEM and EDX analysis.

Declaration of competing interest

The authors declare that they have no known competing financial interests or personal relationships that could have appeared to influence the work reported in this paper.

Data availability

Data will be made available on request.

Acknowledgments

The authors are grateful to the Bangladesh Council of Scientific and Industrial Research (BCSIR) authority for financial support through the approved R&D project.

References

[1] M.S. Hossain, S.M. Tuntun, N.M. Bahadur, S. Ahmed, Enhancement of photocatalytic efficacy by exploiting copper doping in nano-hydroxyapatite for degradation of Congo red dye, RSC Adv. 12 (52) (2022) 34080–34094.
[2] M.P. Das, M. Renuka, J.V. Vijaylakshmi, P.R. Suguna, Removal of methylene blue by adsorption using fish scale chitin, Nat. Environ. Pollut. Technol. 17 (3) (2018) 993–998.
[3] A. Kumar, L. Rout, L.S.K. Achary, S.K. Mohanty, P. Dash, A combustion synthesis route for magnetically separable graphene oxide–CuFe 2 O 4–ZnO nanocomposites with enhanced solar light-mediated photocatalytic activity, New J. Chem. 41 (19) (2017) 10568–10583.
[4] V. Kumar, A.U. Muzaddadi, S. Mann, R. Balakrishnan, K. Bembem, Y. Kalnar, Utilization of Fish Processing Waste, A Waste to Wealth Approach'., 2018.
[5] G. Shanthi, M. Premalatha, N. Anantharaman, Potential utilization of fish waste for the sustainable production of microalgae rich in renewable protein and phycocyanin-Arthrospira platensis/Spirulina, J. Clean. Prod. 294 (2021), 126106.
[6] I.S. Abd Manaf, C.J. Yi, M.H.A. Rahim, G.P. Maniam, Utilization of waste fish bone as catalyst in transesterification of RBD palm oil, Mater. Today: Proc. 19 (2019) 1294–1302.
[7] Y.H. Tan, M.O. Abdullah, J. Kansedo, N.M. Mubarak, Y. San Chan, C. Nolasco-Hipolito, Biodiesel production from used cooking oil using green solid catalyst derived from calcined fusion waste chicken and fish bones, Renew. Energy 139 (2019) 696–706.
[8] P. Terzioğlu, H. Öğüt, A. Kalemtaş, Natural calcium phosphates from fish bones and their potential biomedical applications, Mater. Sci. Eng. C 91 (2018) 899–911.
[9] T.H.A. Corrêa, J.N.F. Holanda, Fish bone as a source of raw material for synthesis of calcium phosphate, Mater. Res. 22 (2019).
[10] P. Govindasamy, et al., Biowaste derived hydroxyapatite embedded on two-dimensional g-C3N4 nanosheets for degradation of hazardous dye and pharmacological drug via Z-scheme charge transfer, Sci. Rep. 12 (1) (2022) 1–16.
[11] S. Mondal, et al., Comparative characterization of biogenic and chemical synthesized hydroxyapatite biomaterials for potential biomedical application, Mater. Chem. Phys. 228 (2019) 344–356.
[12] M. Nurhadi, R. Kusumawardani, I.I. Widiyowati, H. Nur, Utilization of fish bone as adsorbent of Fe3+ ion by controllable removal of its carbonaceous component, in: Journal of Physics: Conference Series, IOP Publishing, 2018, 012031.
[13] P. Shi, M. Liu, F. Fan, C. Yu, W. Lu, M. Du, Characterization of natural hydroxyapatite originated from fish bone and its biocompatibility with osteoblasts, Mater. Sci. Eng. C 90 (2018) 706–712.
[14] N. Muhammad, et al., Extraction of biocompatible hydroxyapatite from fish scales using novel approach of ionic liquid pretreatment, Sep. Purif. Technol. 161 (2016) 129–135.
[15] A. Nayak, B. Bhushan, Hydroxyapatite as an advanced adsorbent for removal of heavy metal ions from water: focus on its applications and limitations, Mater. Today: Proc. 46 (2021) 11029–11034.
[16] S.M.H. Dabiri, A.A. Rezaie, M. Moghimi, H. Rezaie, Extraction of hydroxyapatite from fish bones and its application in nickel adsorption, BioNanoScience 8 (2018) 823–834.
[17] S. Velusamy, A. Roy, S. Sundaram, T. Kumar Mallick, A review on heavy metal ions and containing dyes removal through graphene oxide-based adsorption strategies for textile wastewater treatment, Chem. Rec. 21 (7) (2021) 1570–1610.
[18] S. Sathiyavimal, et al., Facile synthesis and characterization of hydroxyapatite from fish bones: photocatalytic degradation of industrial dyes (crystal violet and Congo red), Prog. Org. Coating 148 (2020), 105890.
[19] A.I. Adeogun, E.A. Ofudje, M.A. Idowu, S.O. Kareem, S. Vahidhabanu, B.R. Babu, Biowaste-derived hydroxyapatite for effective removal of reactive yellow 4 dye: equilibrium, kinetic, and thermodynamic studies, ACS Omega 3 (2) (2018) 1991–2000.
[20] S. Parvin, M.M. Hussain, F. Akter, B.K. Biswas, Removal of Congo red by silver carp (Hypophthalmichthys molitrix) fish bone powder: kinetics, equilibrium, and thermodynamic study, J. Chem. (2021) 1–11, 2021.
[21] M.A.U.R. Al-Kazragi, D.T. Al-Heetimi, Pretreated fishbone as low cost-adsorbent for cationic dye adsorption from aqueous solutions: equilibrium, optimization, kinetic and thermodynamic study, in: Journal of Physics: Conference Series, IOP Publishing, 2021, 022073.
[22] O. Eskikaya, et al., Photocatalytic activity of calcined chicken eggshells for Safranin and Reactive Red 180 decolorization, Chemosphere 304 (2022), 135210.
[23] J. Saha, M.A. Hossain, M.A. Mamun, M.R. Islam, M.S. Alam, Effects of carbon-nitrogen ratio manipulation on the growth performance, body composition and immunity of stinging catfish Heteropneustes fossilis in a biofloc-based culture system, Aquaculture Reports 25 (2022), 101274.
[24] S. Fatma, I. Ahmed, Effect of water temperature on protein requirement of Heteropneustes fossilis (Bloch) fry as determined by nutrient deposition, hemato-biochemical parameters and stress resistance response, Fisheries and Aquatic Sciences 23 (2020) 1–14.
[25] B.N. Paul, S. Chanda, N. Sridhar, G.S. Saha, S.S. Giri, Proximate and mineral composition of magur (Clarias batrachus) and Singhi (Heteropneustes fossilis), Indian J. Anim. Nutr. 32 (4) (2015) 453–456.
[26] N. Shaheen, L. Bari, M.A. Mannan, Food Composition Table for Bangladesh, University of Dhaka, 2013.
[27] M.S. Hossain, M.A.A. Shaikh, M.S. Rahaman, S. Ahmed, Modification of the crystallographic parameters in a biomaterial employing a series of gamma radiation doses, Mol. Syst. Des. Eng., Jun. (2022), https://doi.org/10.1039/D2ME00061J.
[28] Md S. Hossain, M. Mahmud, M.B. Mobarak, S. Sultana, Md A.A. Shaikh, S. Ahmed, New analytical models for precise calculation of crystallite size: application to synthetic hydroxyapatite and natural eggshell crystalline materials, Chem. Pap. (Jul. 2022), https://doi.org/10.1007/s11696-022-02377-9.
[29] M.S. Hossain, M.N. Uddin, S.A. Jahan, S. Ahmed, Synthesis and characterization of nano crystallite plaster of Paris prepared from waste eggshells and exploration of cytotoxicity, hemolysis and antimicrobial properties, J. Mater. Chem. B 11 (2023) 1057–1067.
[30] A. Monshi, M.R. Foroughi, M.R. Monshi, Modified Scherrer equation to estimate more accurately nano-crystallite size using XRD, World J. Nano Sci. Eng. 2 (3) (2012) 154–160.
[31] N.T. Tayade, M.P. Tirpude, Frustrated microstructures composite PbS material's size perspective from XRD by variant models of Williamson–Hall plot method, Bull. Mater. Sci. 46 (1) (2023) 20.
[32] D. Jamwal, G. Kaur, P. Raizada, P. Singh, D. Pathak, P. Thakur, Twin-tail surfactant peculiarity in superficial fabrication of semiconductor quantum dots: toward structural, optical, and electrical features, J. Phys. Chem. C 119 (9) (2015) 5062–5073.
[33] A. Velazquez-Palenzuela, et al., Structural properties of unsupported Pt- Ru nanoparticles as anodic catalyst for proton exchange membrane fuel cells, J. Phys. Chem. C 114 (10) (2010) 4399–4407.
[34] S.D. Lala, E. Barua, P. Deb, A.B. Deoghare, Physico-chemical and biological behaviour of eggshell bio-waste derived nano-hydroxyapatite matured at different aging time, Mater. Today Commun. 27 (2021), 102443.